Article

Lithiophilic Quinone Lithium Salt Formed by Tetrafluoro-1,4-Benzoquinone Guides Uniform Lithium Deposition to Stabilize the Interface of Anode and PVDF-Based Solid Electrolytes

Yinglu Hu [1], Li Liu [1], Jingwei Zhao [2,*], Dechao Zhang [1], Jiadong Shen [1], Fangkun Li [1], Yan Yang [1], Zhengbo Liu [1], Weixin He [1], Weiming Zhao [1] and Jun Liu [1,*]

[1] Guangdong Provincial Key Laboratory of Advanced Energy Storage Materials, School of Materials Science and Engineering, South China University of Technology, Guangzhou 510641, China

[2] Research and Development Center, Guangzhou Tinci Materials Technology Co., Ltd., Guangzhou 510765, China

* Correspondence: zhaojingwei@tinci.com (J.Z.); msjliu@scut.edu.cn (J.L.)

Abstract: Poly(vinylidene fluoride) (PVDF)-based composite solid electrolytes (CSEs) are attracting widespread attention due to their superior electrochemical and mechanical properties. However, the PVDF has a strong polar group -CF_2-, which easily continuously reacts with lithium metal, resulting in the instability of the solid electrolyte interface (SEI), which intensifies the formation of lithium dendrites. Herein, Tetrafluoro-1,4-benzoquinone (TFBQ) was selected as an additive in trace amounts to the PVDF/Li-based electrolytes. TFBQ uniformly formed lithophilic quinone lithium salt (Li_2TFBQ) in the SEI. Li_2TFBQ has high lithium-ion affinity and low potential barrier and can be used as the dominant agent to guide uniform lithium deposition. The results showed that PVDF/Li-TFBQ 0.05 with a mass ratio of PVDF to TFBQ of 1:0.05 had the highest ionic conductivity of 2.39×10^{-4} S cm^{-1}, and the electrochemical stability window reached 5.0 V. Moreover, PVDF/Li-TFBQ CSE demonstrated superior lithium dendrite suppression, which was confirmed by long-term lithium stripping/sedimentation tests over 2000 and 650 h at a current of 0.1 and 0.2 mA cm^{-2}, respectively. The assembled solid-state $LiNi_{0.6}Co_{0.2}Mn_{0.2}O_2$||Li cell showed an excellent performance rate and cycle stability at 30 °C. This study greatly promotes the practical research of solid-state electrolytes.

Keywords: solid-state lithium battery; polymer electrolytes; solid electrolytes interface; poly(vinylidene fluoride)

1. Introduction

Lithium-ion batteries (LIBs) are indispensable energy storage devices in daily life and are widely used in many fields, and the increasing demand in applications has promoted research on LIBs with high power/energy density and good safety [1,2]. Almost all LIBs usually use organic electrolytes as ion-conducting media in practical applications; their flammability brings great challenges to the safety of LIBs. Meanwhile, uneven lithium deposition and huge volume effect cause the rupture of the SEI layer and the growth of lithium dendrites, which will reduce the coulomb efficiency and battery life, limiting the increase in energy density [3–5]. The development and use of solid-state electrolytes can effectively alleviate these problems and offer possibilities for the development of solid-state lithium metal batteries [6].

Solid electrolytes are generally classified into three categories [7]: inorganic solid electrolytes, solid polymer electrolytes (SPEs), and composite solid electrolytes (CSEs). For inorganic solid electrolytes, studies of $Li_7La_3Zr_2O_{12}$ (LLZO) [8], $Li_{1-x}Al_xTi_{2-x}(PO_4)_3$

(LATP) [8], $Li_{10}GeP_2S_{12}$ (LGPS) [9], e.g., have been reported. For SPEs, polyethylene oxide (PEO) [6], poly(vinylidene fluoride) (PVDF) [10], polyvinylidene fluoride hexafluoropropylene (PVDF-HFP) [11], polyacrylonitrile (PAN) [12] and polymethylmethacrylate (PMMA) [13], e.g., can be used as polymer matrices. Through component control and structural design, composite solid electrolytes (CSEs) that combine the advantages of different types of electrolytes can improve the overall ionic conductivity and mechanical strength. Common composite solid electrolytes include polymers and inorganic fillers [14], polymers and polymers [15], and other synergistic approaches. Polymer electrolytes are commonly used as matrices, and inorganic fillers play the role of effectively reducing the crystallinity of polymer matrices, expanding amorphous regions, and increasing the content of free Li^+ to improve ionic conductivity [16,17].

PVDF has the advantages of good mechanical properties, non-flammability, strong solubility of lithium salts and low price, so it is very suitable for use as a polymer matrix for composite electrolytes [18]. However, PVDF polymer also has obvious shortcomings in lithium battery research applications; first of all, high crystallinity at room temperature brings excellent mechanical properties but also hinders the improvement in the ion conductivity. Secondly, the incompatibility of PVDF polymer and lithium metal, PVDF has a strong polar group -CF_2-, lithium metal reacts easily with PVDF and causes the instability of the contact interface [19,20]. Through extensive attempts and in-depth exploration, it is scientific and feasible to modify PVDF-based solid electrolytes with different design strategies. Modification using inorganic fillers can significantly enhance ion conductivity, mechanical properties, and thermal stability. Zhang et al. [21] used LLZTO as the active filler in the PVDF-HFP polymer matrix, making lithium salt LiFSI more easily dissociated and providing more migration Li^+; LLZTO can provide additional Li^+ migration paths, effectively improving the electrochemical stability of solid-state electrolyte. Li et al. [22] prepared a solid polymer electrolyte with PVDF, using CA (cellulose acetate) as the matrix and modified MMT (montmorillonite) as a filler; CA promoted the sufficient spatial conformation of the polymer molecular segment so Li^+ could be transferred conveniently, improved the mechanical strength of the membrane, and restrained the growth of lithium dendrites. Zeng et al. [23] enhanced the polarization of polymers by copolymerizing trifluoro-ethylene (TrFE) monomer with PVDF monomer and exhibiting the pure all-trans (TTTT) planar zigzag conformation at the TrFE content of 20 to 50 mol%, thereby achieving an improvement in ionic conductivity. Liu et al. [24] used PVDF-HFP as the matrix, through ingenious structural design, to create a novel type of polymer-in-salt solid electrolyte (PISSE), which can penetrate and grow directly in the three-dimensional (3D) electrode on the current collector spacing to achieve the most adequate contact between the electrode and the solid polymer electrolyte.

Like most solid electrolytes, the interface problem of PVDF-based solid electrolytes remains unresolved, and uneven lithium ion conductivity leads to uneven nucleation of lithium deposition, exacerbating the formation of lithium dendrites [25]. Higher current densities result in more susceptible breakage of the SEI, and the fresh lithium metal exposed under the crack has a lower lithium ion transport barrier, which in turn leads to more uneven lithium deposition [26], which may lead to low coulomb efficiency, short long-term operation cycle, and other safety hazards. It greatly affects the improvement in battery energy density and battery safety [27,28]. Therefore, the SEI layer is crucial to the overall performance of lithium metal anodes and lithium batteries; it regulates the current distribution during lithium deposition by changing the physicochemical properties, thereby fundamentally inhibiting the production of lithium dendrites.

The original SEI layer usually exhibits fragile characteristics, and the method of in situ formation can be regarded as the most feasible, practical and constructive, showing outstanding lithium dendrite inhibition ability and promoting the circulation of lithium metal electrodes [29]. The lithiophilic matrix of the SEI layer reduces the potential barrier for lithium nucleation, balances the current distribution, and enhances the binding of lithium ions to other substances. Qian et al. reported an electrolyte additive in lithium

metal batteries: tetrachloro-1,4-benzoquinone (TCBQ) and found through experiments that its decomposition product (Li_2TCBQ) in SEI is more lithiophilic [30]. Specifically, TCBQ can be neatly stacked and arranged between molecules because of its unique chemical bonds, and lithium ions are neatly riveted on the surface of TCBQ, and the formed Li_2TCBQ, LiF, and Li_2CO_3 together form a stable SEI layer [31]. It can be seen that benzoquinone based on conjugated carbonyl compounds has excellent performance in reaction kinetics, combined with stable amorphous structure, which is very valuable in the selection of electrolyte additives. As a similar substance, tetrafluoro-1,4-benzoquinone (TFBQ) contains F-groups that are more competitive than TCBQ, and the effect of micro-addition plays a significant role and can be utilized as the high-potential additive for composite electrolyte modification.

Therefore, in this study, PVDF was selected as the polymer matrix, a high-concentration of lithium salt (LiTFSI) was added, and TFBQ was selected as the additive, in the hopes that a trace amount of TFBQ added to the PVDF/Li-based electrolyte could uniformly form a new lithiophilic quinone lithium salt (Li_2TFBQ) component in the SEI layer. Due to its strong lithium-ion affinity and relatively low potential barrier, Li_2TFBQ can be used as a guiding agent of SEI layer to promote uniform lithium deposition. This has been proven in this experiment through related physicochemical performance characterization and electrochemical testing. PVDF-based composite solid electrolytes with trace TFBQ have excellent stability coupled to symmetric lithium electrodes, and under the current density gradient of 0.1–0.4 mA cm^{-2}, lithium symmetric cells can stabilize the cycle with stable polarization voltage and without short circuits. In addition, the PVDF/Li-TFBQ CSE confirmed the significant suppression of lithium dendrite growth through long-term lithium stripping/deposition tests for more than 200 h. It was worth emphasizing that the assembled solid-state $LiNi_{0.6}Co_{0.2}Mn_{0.2}O_2$||Li cells exhibited excellent rate performance and cycle stability at 30 °C. In this experiment, the effect of trace benzoquinone additives on the anode interface of composite solid electrolytes was explored, opening up a new idea for the modification of solid electrolyte interfaces.

2. Materials and Methods

2.1. Material Synthesis

In this work, through the solution casting method of synthesized PVDF/Li-TFBQ CSEs membranes: First, polyvinylidene fluoride (PVDF, HF-Kejing, Hefei, China), lithium bis(trifluoromethane sulfonyl)imide (LiTFSI, 99.99%, Sigma-Aldrich, St. Louis, MI, USA), and a certain amount of tetrafluoro-1,4-benzoquinone (TFBQ, Sigma-Aldrich) were dissolved in N, N-dimethylformamide (DMF, 99.8%, Sigma-Aldrich) solution. Next, we stirred the obtained solution continuously at 60 °C for 12 h to form a homogeneous solution. Then, we evenly coated the slurry on the clean polytetrafluoroethylene(PTFE) mold and placed it horizontally to be evaporated and shaped and vacuum-dried at 80 °C for 12 h to obtain a membranes thickness of about 100 μm. In subsequent characterization and testing, the electrolyte membranes were cut to the appropriate size as required (the diameter of all electrolyte membranes assembled into the button cell was 16 mm).

2.2. Preparation of LiNi$_{0.6}$Co$_{0.2}$Mn$_{0.2}$O$_2$ Cathodes

The components of the cathode are $LiNi_{0.6}Co_{0.2}Mn_{0.2}O_2$ powder, poly(vinylidene fluoride) (PVDF), and carbon black (super P); the three components were added to the N-methyl pyrrolidone (NMP) solution in the mass ratio of 8:1:1 and stirred vigorously, the obtained slurry was coated on aluminum foil, and vacuum-heated at 80 °C for 12 h, and then cut into small discs with the diameter of 12 mm, and the average mass loading of the active material on the cathode is approximately 2.0–2.3 mg cm^{-2}.

2.3. Material Characterization

The purity of the samples was identified by XRD, and the crystallinity changes of the composite electrolyte membranes were analyzed with a test angle of 10–70% and a test step size of 0.010 (Cu K$_\alpha$ radiation). The micro-morphology and thickness measurements of

the composite electrolyte membranes were analyzed by SEM and EDS, and the electrode materials before and after cycling were also micro-characterized. Electrolyte membranes stability was analyzed by thermogravimetric analysis (TGA). The change of melting temperature point (T_m) of the composite electrolyte was analyzed by DSC, and then the change of crystallinity was reflected. The heating rate was 10 °C min^{-1}, the test temperature range was 70–200 °C, and the protective atmosphere was argon atmosphere. The transformation of the chemical bond of the samples were characterized by Fourier transform infrared spectroscopy (FTIR), and the test wavelength range was 4000–600 cm^{-1}. The interface between the electrolyte and the lithium metal anode was tested by XPS on a Thermo K-Alpha XPS spectrometer equipped with a monochromatic Al-K$_\alpha$ X-ray source to analyze the composition and content change of the main phase substances in the interface layer.

2.4. Electrochemical Measurements

The ionic conductivity of electrolytes in the stainless steel (SS)||CSE||SScell was measured by Electrochemical impedance spectroscopy (EIS) in the temperature range of 10–80 °C with alternating current (AC) amplitude of 0.01 V and frequency range of 1–106 Hz. The linear sweep voltammetry (LSV) of the electrolyte was tested by Li||CSE Licell with a voltage range of 2–6 V and a scan rate of 0.001 V s^{-1}. The lithium-ion transference number (t_{Li+}) of the electrolyte was calculated from direct current polarization and alternating current impedance measurements using Li||CSE||SS cells at 25 °C. At 30 °C, the electrochemical properties of all lithium symmetric cells Li||CSE||SS and $LiNi_{0.6}Co_{0.2}Mn_{0.2}O_2$||Li solid-state cell were measured by the LAND charge–discharge test system. All cells were assembled into CR 2025 coin cells in a glove box filled with argon gas with lithium metal foil as the anode, using only CSE as the electrolyte and no liquid electrolyte added.

3. Results

In this work, PVDF/Li-TFBQ CSE membranes were synthesized via solution casting method, and a series of PVDF/Li-TFBQ samples with different additive contents were prepared; the mass ratio of PVDF to LiTFSI was 1:1.25, and the mass ratio of PVDF to additive TFBQ were 1:0.1, 1:0.05, and 1:0.01, respectively, named PVDF/LiTFSI, PVDF/Li-TFBQ 0.1, PVDF/Li-TFBQ 0.05, and PVDF/Li-TFBQ 0.01, respectively, in which the PVDF/LiTFSI was the control test group without any additives.

The X-ray diffraction (XRD) pattern of Figure 1a shows the phase and crystallinity of LiTFSI, TFBQ, and PVDF/Li-TFBQ CSE membranes. After adding LiTFSI and TFBQ, the characteristic peaks of PVDF at 20° and 40° showed a decrease in diffraction peak intensity, and the position of the diffraction peak did not shift, indicating that the degree of the amorphous state of PVDF was strengthened after mixing with lithium salt and additives. This shows that the addition of TFBQ additive and LiTFSI can increase the amorphous region of the PVDF matrix and reduce crystallinity. At the same time, in the composite electrolyte, neither lithium salt nor additive shows their corresponding characteristic peaks, which indicates that the lithium salt and additive added to the system were homogeneously mixed with the PVDF matrix rather than in a dispersed form. As shown in Figure 1b, the crystallinity of PVDF decreases with the addition of LiTFSI and TFBQ by analyzing the differential scanning calorimetry (DSC) curves of pure PVDF, PVDF/LiTFSI, and PVDF/Li-TFBQ membranes. The endothermic peak of the pure PVDF membranes appeared at 154 °C, that is, the crystalline-amorphous transition temperature (T_m). Due to ensuring the appropriate usage of LiTFSI, the endothermic peak of the electrolyte obviously decreased to 148 °C and decreased more significantly with the addition of TFBQ, which also proved that the addition of LiTFSI and TFBQ could effectively reduce the crystallinity of PVDF polymer, among which PVDF/Li TFBQ 0.05 showed the lowest endothermic peak temperature of 130 °C, which means that there were more amorphous regions in this sample, which is more conducive to the formation of lithium ions. In order to further explore the effect of additives and lithium salts on the composite electrolyte, the chemical bond transition

of these samples was investigated by FTIR spectroscopy. In the FTIR spectra shown in Figure 1c, the characteristic peaks of 761 and 1402 cm^{-1} correspond to the α-phase crystals, and the characteristic peaks of 835 and 876 cm^{-1} correspond to the amorphous phases. It is worth noting that the absorption peaks of -CF$_2$-, located at 1072 and 1171 cm^{-1}, were shifted after adding LiTFSI, and a new absorption peak was also generated at 1660 cm^{-1} due to the interaction between the PVDF matrix and LiTFSI. The amorphous phase peak at 876 cm^{-1} also weakened in intensity after adding TFBQ, which corresponds well to the results of DSC and XRD. At the same time, a new characteristic peak appeared at 957 cm^{-1} in the experimental group samples, which strengthens with the increase in additive addition, which is the characteristic peak of the C-F bond in TFBQ, which indicates that the TFBQ additive is successfully mixed inside the composite electrolyte.
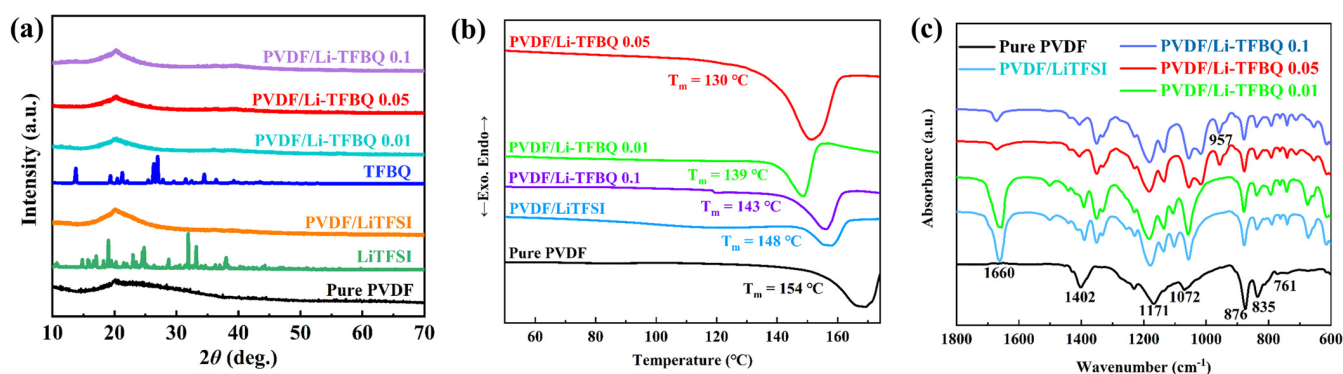

Figure 1. (**a**) X-ray diffraction (XRD) patterns of TFBQ, LiTFSI, pure PVDF, PVDF/Li, and PVDF/ Li-TFBQ CSE membranes, DSC profiles (**b**) and FTIR spectra (**c**) of pure PVDF, PVDF/Li, and PVDF/Li-TFBQ CSE membranes.

To explore the appropriate amount of TFBQ, we measured the ionic conductivity of different samples at room temperature, as shown in Figure 2a,b, PVDF/Li-TFBQ 0.05 showed the highest ionic conductivity (2.39 × 10^{-4} S cm^{-1}) at 25 °C after multiple tests and calculations with the same repeatability. To further verify the scientific conclusion, we also tested and summarized the ionic conductivity performance at different temperatures; as shown in Figure 2c, it can be clearly found that PVDF/Li-TFBQ 0.05 has the highest ionic conductivity at different temperature points in the entire temperature range. According to the approximate slope of its curve, it can also be seen that the sample has a low ionic migration barrier. Therefore, PVDF/Li-TFBQ 0.05 was the optimal sample according to the performance of ionic conductivity; that is, when the mass ratio of PVDF to TFBQ was 1:0.05, it was the optimal micro-addition amount of additive, and subsequent characterization and testing were carried out on this sample.

To characterize the thermal stability of the composite electrolyte, the thermo-gravimetric loss of the electrolyte membranes was detected in the temperature range of 40–700 °C by TG, as shown in Figure 2d, after adding lithium salt and TFBQ, the thermal stability of CSE is not destroyed, it still has excellent thermal stability in a wide temperature range as the pure phase PVDF membranes, indicating that the PVDF/Li-TFBQ 0.05 CSE membranes also have better safety performance.

In addition to being expected to play a positive role at the electrolyte interface, the additive TFBQ can also facilitate the dissociation of LiTFSI and improve the ionic conductivity, as demonstrated in additive exploration experiments. At the same time, whether the dissociation of lithium salt is further facilitated can also be reflected by the number of electrolyte ions. Therefore, the results of the lithium-ion migration number test and calculation of the sample are shown in Figure 2e, the lithium-ion migration number of PVDF/Li-TFBQ 0.05 at room temperature can reach 0.42, which is much higher than the ion migration number of ordinary PVDF-based composite solid electrolytes (about 0.3), which further confirms that the addition of TFBQ can facilitate the dissociation of LiTFSI

and upgrade the overall electrochemical performance of the composite solid electrolyte. To characterize the adaptability of the composite solid electrolyte to the cathode material, the electrolyte samples were tested for LSV to characterize the electrochemical stability window, and the results are shown in Figure 2f; the overall electrochemical stability of the composite solid electrolyte also improved after TFBQ addition, and the electrochemical window of the PVDF/Li-TFBQ 0.05 reached 5.0 V, possibly because TFBQ not only promoted the dissociation of lithium salt but also made the distribution of lithium salt more uniform and also absorbed some impurities in the electrolyte as a cross-linking center, thus improving overall antioxidant resistance.
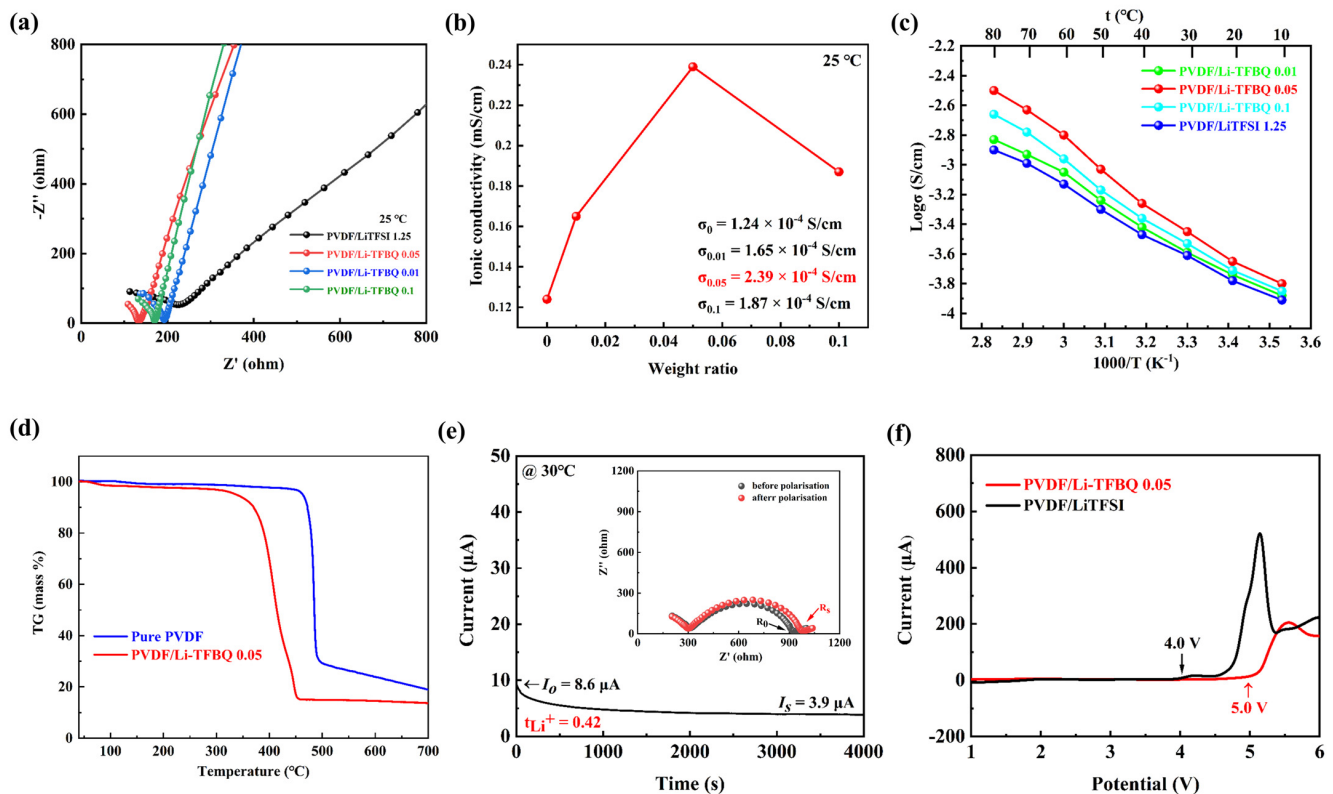

Figure 2. Impendence spectra (**a**) and ionic conductivities (**b**) of PVDF/Li-TFBQ CSE membranes with different contents of TFBQ at room temperature, (**c**) Arrhenius plots of ionic conductivities of PVDF/Li and PVDF/Li-TFBQ CSE membranes. (**d**) TG curves of pure PVDF and PVDF/Li-TFBQ 0.05 CSE membranes. (**e**) Direct current polarization result for the Li||PVDF/Li-TFBQ 0.05||Li symmetrical cell and its EIS variation before and after polarization (inset), (**f**) linear sweep voltammetry plot of PVDF/Li and PVDF/Li-TFBQ 0.05 CSE membranes at 25 °C.

The interfacial compatibility and stability of electrolyte and lithium metal have great influence on cell performance. To directly demonstrate the contact stability between lithium metal and electrolyte, the EIS experiment of the lithium-symmetric cell was designed, and then the interface compatibility and stability of PVDF/Li-TFBQ 0.05 CSE and lithium electrode after long-term contact between the electrolyte membranes and lithium metal at room temperature was analyzed. As shown in Figure 3a, the interface between the CES membranes and lithium metal tends to balance and stabilize after three days of contact, with no significant increase in interface resistance, indicating good interface stability. The electrochemical stability of the CSE under high voltage was further evaluated by applying a constant voltage of 4.5 V to the cell for 150 h and performing impedance measurements. Figure 3b shows Li||PVDF/Li-TFBQ 0.05||SS asymmetric cell impedance spectrum over time. Through the analysis of experimental results, the almost constant resistance at constant voltage proves the significant electrochemical stability of CSE. The stability of long-term battery cycling is significantly affected by the interface state between the

electrolyte and the lithium metal electrode, so the deposition/stripping process of the lithium symmetric battery was analyzed to evaluate the stability between the electrolyte and the lithium metal anode. Figure 3c shows the rate performance of lithium-symmetric cells for different current magnitudes at room temperature. Under the current density gradient of 0.1–0.4 mA cm^{-2}, lithium-symmetric cells can cycle stably with stable polarization voltage and no short circuit. In addition, as shown in Figure 3d,e, PVDF/Li-TFBQ CSE shows outstanding lithium dendrite suppression ability, which can stably cycle for more than 2000 and 650 cycles, respectively, under the current of 0.1 and 0.2 mA cm^{-2}, and the voltage polarization change is small before, during, and after the cycle, which indicates that the interface condition between the electrolyte and lithium metal remains stable throughout the cycle. It can be seen that the addition of TFBQ can improve the interfacial stability of electrolyte and lithium metal.
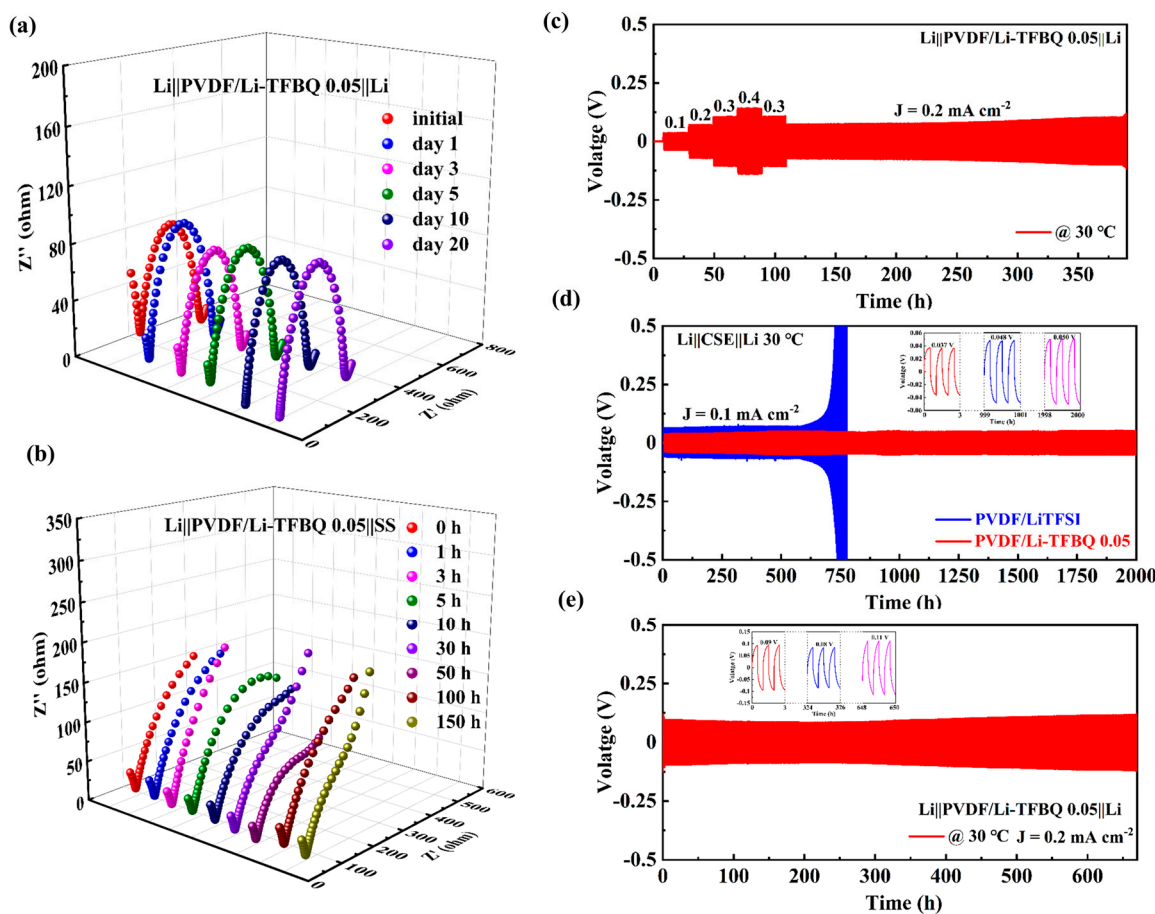

Figure 3. (**a**) Impedance spectra of Li‖PVDF/Li-TFBQ 0.05‖Li symmetrical cell for different aging times. (**b**) Impedance spectra of Li‖PVDF/Li-TFBQ 0.05‖SS unsymmetrical cell at bias voltage 4.5 V. (**c**) Galvanostatic rate performance of the Li symmetrical cell with a current density of 0.1–0.3 mA cm^{-2} at 30 °C. Galvanostatic long-term cycling of Li‖PVDF/Li-TFBQ 0.05‖Li symmetrical cell with a current density of 0.1 mA cm^{-2} (**d**) and 0.2 mA cm^{-2} (**e**).

The microscopic morphology of the electrolyte can be intuitively analyzed through SEM images. Due to the absence of inorganic fillers, the PVDF/Li TFBQ 0.05 CSE membranes have a smoother and more uniform surface, as shown in Figure 4a,b, which can bring positive effects on the ion transport inside the electrolyte and the stability of the interface between the electrolyte and the electrode. At the same time, as shown in Figure 4c, the cross-section shows that the thickness of the electrolyte is about 100 μm. The thinner electrolyte shows that the migration path of lithium ions is shortened during cell operation, which has a positive significance for reducing cell polarization and improving the ionic

conductivity of the electrolyte. The thinner thickness of the electrolyte is an encouraging sign for the application of all solid-state batteries. The EDS analysis provides insight into the distribution of various elements inside the electrolyte. As shown in Figure 4d–g, N, F, S, and O are characteristic elements of LiTFSI, and it can be intuitively found that various elements are uniformly distributed in the electrolyte section, which indicates that although the composite electrolyte is added with high concentrations of lithium salts, it is still completely dissolved and evenly distributed inside the electrolyte matrix. It can be seen that the simple solution casting method can also obtain high-quality electrolyte membranes with uniform composition and smooth morphology.
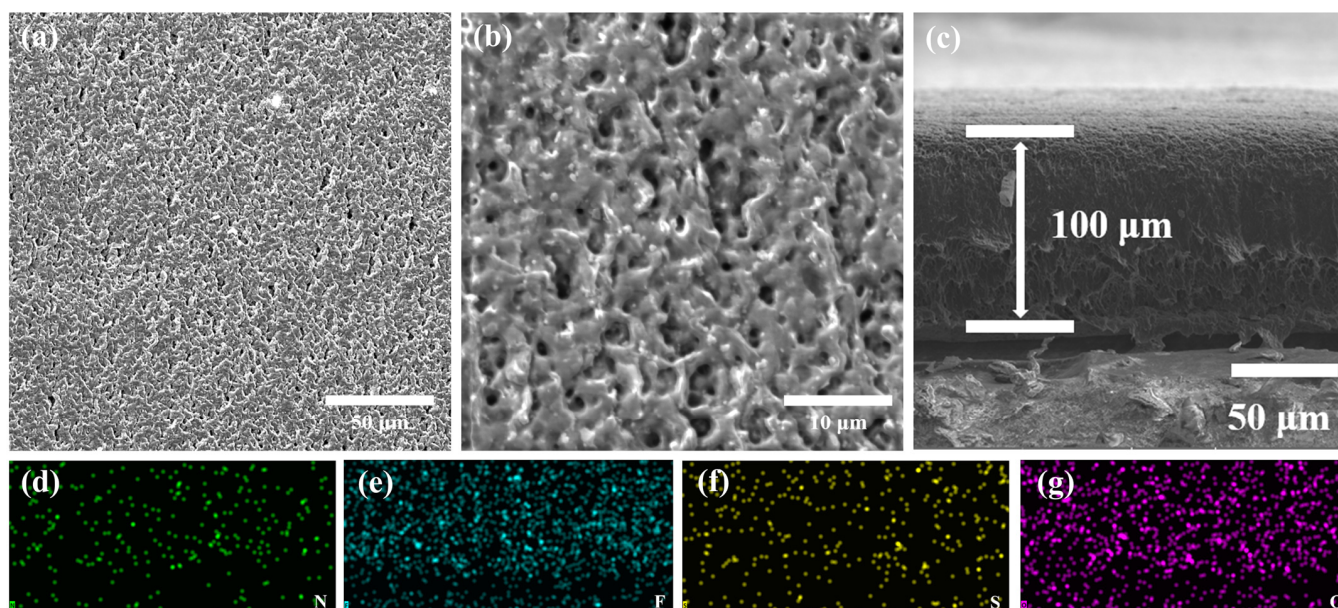

Figure 4. Surface (**a**,**b**) and cross-sectional (**c**) SEM images of PVDF/Li-TFBQ 0.05 CSE membranes, corresponding EDS mapping of nitrogen (**d**), fluorine (**e**), sulfur (**f**), and oxygen (**g**).

The lithium metal interface of Li | | PVDF/LiTFSI | | Li and Li | | PVDF/Li-TFBQ 0.05 | | Li symmetrical cell after 100 cycles at 0.1 mA cm^{-2} current were analyzed by SEM images. As shown in Figure 5c,d, after contact with PVDF/LiTFSI electrolyte membranes and deposition/stripping 100 times, the surface of the lithium metal electrode plate obviously shows uneven lithium deposition, which is characterized by rough and loose interface and irregular lithium dendrites. In contrast, the surface of the lithium metal electrode after PVDF/Li-TFBQ 0.05 CSE contact, shown in Figure 5a,b, is flatter and smoother, and no lithium dendrite is observed. This indicates that lithium-ions are deposited more uniformly on the surface, which also confirms our assumption that the TFBQ additive can spontaneously form a stable SEI layer on the surface of lithium metal and guide the uniform deposition of lithium ions. To further verify the influence of TFBQ additive on the interface layer of electrolyte and lithium metal, we performed in situ XPS characterization on the lithium metal surface of the lithium symmetric cell after cycling to determine the chemical composition information in the electrochemical process. Figure 5e shows the XPS spectra of F, O, and C elements. After the addition of TFBQ, a more stable interface layer mainly composed of LiF, Li$_2$CO$_3$, and Li$_2$TFBQ was formed on the lithium anode due to the interface reaction between TFSI$^-$ and TFBQ and lithium metal, providing good ion conductivity. At the same time, electronic insulation and mechanical properties were improved, thereby achieving the suppression of side reactions and uniform lithium deposition/stripping.
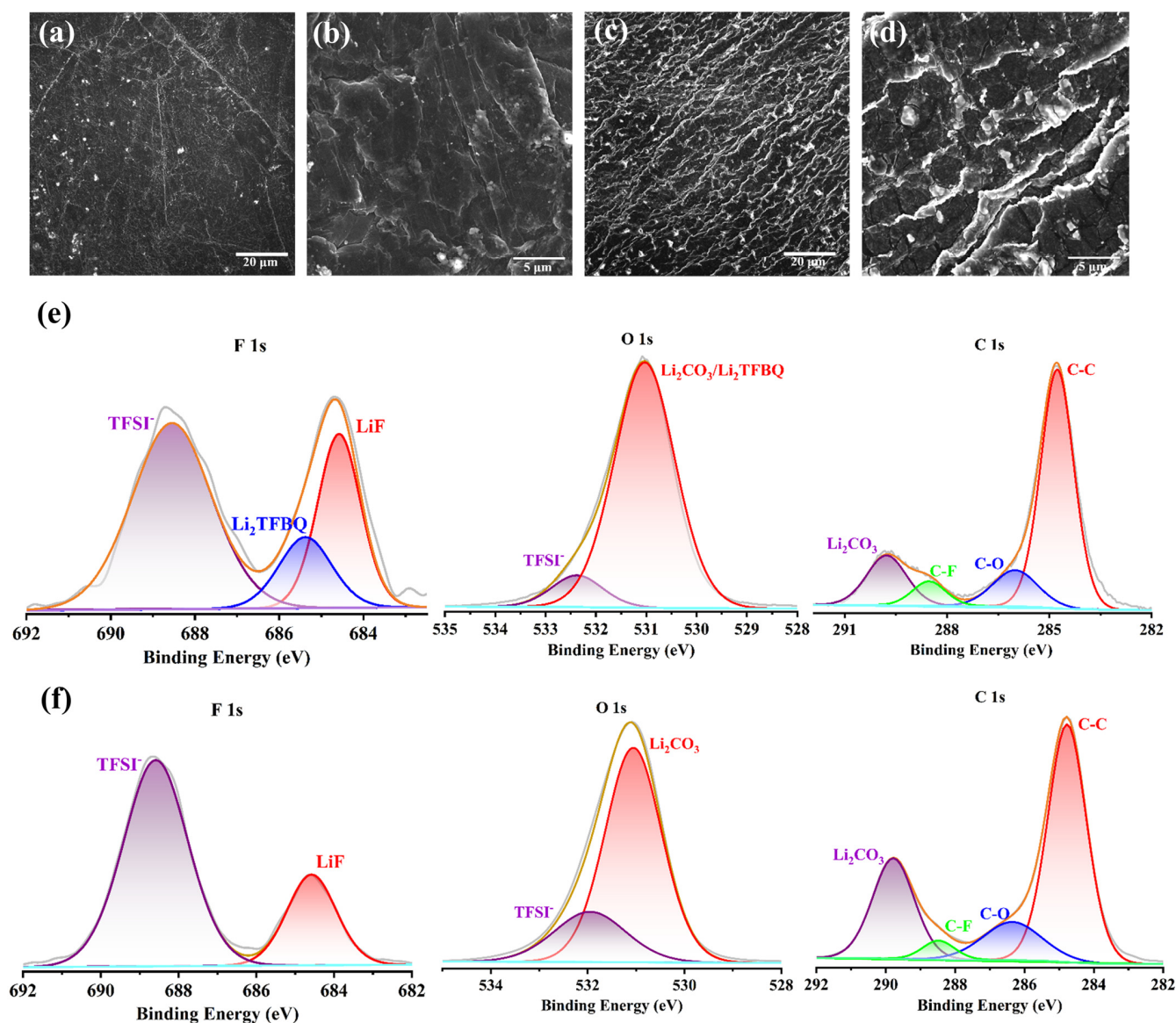
Figure 5. SEM images and XPS spectra of cycled Li metal collected from symmetrical Li cells utilizing PVDF/Li-TFBQ 0.05 (**a**,**b**,**e**) and PVDF/Li (**c**,**d**,**f**).

To verify the performance of the PVDF/Li-TFBQ 0.05 composite electrolyte cell, we assembled solid $LiNi_{0.6}Co_{0.2}Mn_{0.2}O_2$ ‖ Li button cells and tested the rate and cycle performance of the cells at 30 °C. As shown in Figure 6a, at currents of 0.2, 0.3, 0.5, 1, and 1.5 C, the cells show good discharge specific capacities of 160, 152, 140, 110, and 90 mA h g^{-1}, respectively, which is comparable to the rate performance of most conventional electrolyte cells. The charge–discharge curve of these cells is shown in Figure 6d. Under the current condition of low rate, the voltage polarization is small, while under the condition of high rate, although the polarization is increased, it can still maintain a high-capacity performance. As shown in Figure 6b, in the long-term cycle of the cell, the capacity of nearly 150 mA h g^{-1} can be kept stable for more than 180 cycles under a current of 0.2 C, the capacity retention rate is more than 80%, and the coulomb efficiency also remains at a high level during the cycle. According to the charge–discharge curve in Figure 6e, the capacity of the cell gradually increased to the highest level within the first 50 cycles. The reason is that there is a homogenization process in the initial charge–discharge cycle of the cell, and the internal ion conduction and interface contact conditions of the cell gradually stabilize with the progression of the charge–discharge cycle. As

shown in Figure 6e,f, $LiNi_{0.6}Co_{0.2}Mn_{0.2}O_2$ | | Li cell can stably cycle the capacity of nearly 125 mA h g^{-1} for about 100 cycles under a current of 0.5 C, and the capacity retention rate can also reach 65% after 300 cycles and maintain a high coulomb efficiency of nearly 100% in the whole process. It can also be seen from the charge–discharge curve of the cell that voltage polarization is large during the high-current cycle, but it is worth affirming that the cell can still guarantee high-quality capacity output in the first 100 cycles, which is of positive significance to the research of solid-state high-voltage high-capacity lithium batteries. Through the test of $LiNi_{0.6}Co_{0.2}Mn_{0.2}O_2$ | | Li cell assembled by PVDF/Li-TFBQ 0.05 composite electrolyte, it can be seen that the electrolyte ensures the overall excellent multiple and cycle performances of the cell with its good electrochemical performance. In a word, the cell performance of PVDF-based composite electrolyte can be significantly improved by adding the appropriate amount of TFBQ.
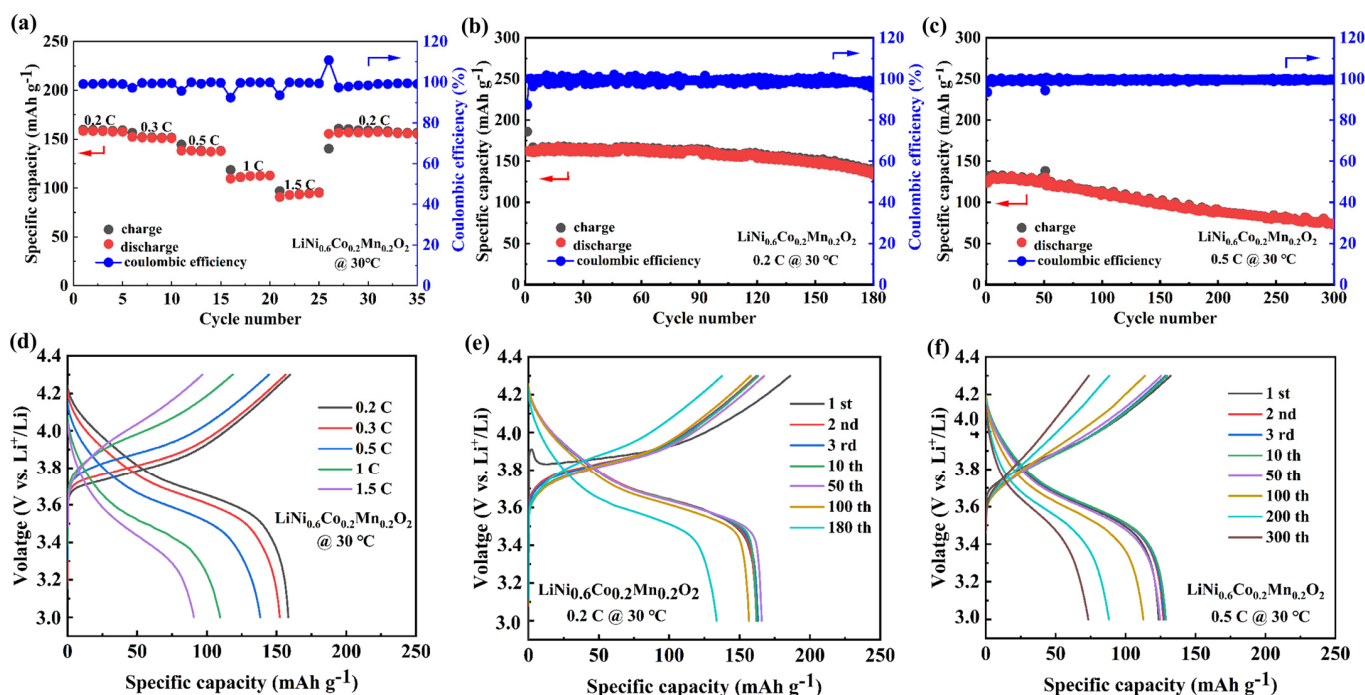

Figure 6. (**a**) Rate performance at rates of 0.2–1.5 C of $LiNi_{0.6}Co_{0.2}Mn_{0.2}O_2$ cells. (**b,c**) Cycling performance of cells at different rates. (**d–f**) Selective charge–discharge curves after different cycles of cells at different rates, cycled at 30 °C.

4. Conclusions

In summary, the addition of benzoquinone additive TFBQ to PVDF-based composite electrolytes can promote the uniform deposition of lithium. In the electrochemical process, due to its unique chemical bonds, the molecules can be neatly stacked and arranged, and it has strong lithiophilicity, and then lithium-ions are neatly riveted on the surface of TFBQ. That is, a small amount of TFBQ in the electrolyte can be sacrificed and decomposed to form a uniform Li_2TFBQ layer in the SEI layer on the surface of the Li anode. This component exhibits a relatively low energy barrier, thus effectively improving the stability of the lithium metal anode surface by regulating the deposition of lithium metal, thereby further reducing the side reaction resistance between the electrolyte and lithium metal. The results show that the lithium symmetrical cell assembled with the electrolyte containing an appropriate amount of TFBQ can cycle stably under the condition of stable polarization voltage and no short circuit under the current density gradient of 0.1–0.4 mA cm^{-2}. In addition, PVDF/Li TFBQ CSE exhibits outstanding lithium dendrite suppression ability, which has been demonstrated by long-term lithium stripping/deposition tests conducted at currents of 0.1 and 0.2 mA cm^{-2} for over 2000 and 650 h, respectively. The solid $LiNi_{0.6}Co_{0.2}Mn_{0.2}O_2$ | | Li cell assembled with the CSE also shows outstanding rate and

cycling performance at room temperature. Therefore, TFBQ is a promising additive in the composite solid electrolyte system.

References

1. Li, M.; Lu, J.; Chen, Z.; Amine, K. 30 Years of Lithium-Ion Batteries. *Adv. Mater.* **2018**, *30*, 1800561. [CrossRef] [PubMed]
2. Chen, S.; Wen, K.; Fan, J.; Bando, Y.; Golberg, D. Progress and future prospects of high-voltage and high-safety electrolytes in advanced lithium batteries: From liquid to solid electrolytes. *J. Mater. Chem. A* **2018**, *6*, 11631–11663. [CrossRef]
3. Zheng, L.; Zhang, H.; Cheng, P.; Ma, Q.; Liu, J.; Nie, J.; Feng, W.; Zhou, Z. $Li[(FSO_2)(n-C_4F_9SO_2)]N$ versus $LiPF_6$ for graphite/$LiCoO_2$ lithium-ion cells at both room and elevated temperatures: A comprehensive understanding with chemical, electrochemical and XPS analysis. *Electrochim. Acta* **2016**, *196*, 169–188. [CrossRef]
4. Kalhoff, J.; Eshetu, G.G.; Bresser, D.; Passerini, S. Safer Electrolytes for Lithium-Ion Batteries: State of the Art and Perspectives. *ChemSusChem* **2015**, *8*, 2154–2175. [CrossRef]
5. Yang, C.; Fu, K.; Zhang, Y.; Hitz, E.; Hu, L. Protected Lithium-Metal Anodes in Batteries: From Liquid to Solid. *Adv. Mater.* **2017**, *29*, 1701169. [CrossRef]
6. Wu, F.; Maier, J.; Yu, Y. Guidelines and trends for next-generation rechargeable lithium and lithium-ion batteries. *Chem. Soc. Rev.* **2020**, *49*, 1569–1614. [CrossRef]
7. Murugan, R.; Thangadurai, V.; Weppner, W. Fast Lithium Ion Conduction in Garnet-Type $Li_7La_3Zr_2O_{12}$. *Angew. Chem. Int. Ed.* **2007**, *46*, 7778–7781. [CrossRef] [PubMed]
8. Epp, V.; Ma, Q.; Hammer, E.-M.; Tietz, F.; Wilkening, M. Very fast bulk Li ion diffusivity in crystalline $Li_{1.5}Al_{0.5}Ti_{1.5}(PO_4)_3$ as seen using NMR relaxometry. *Phys. Chem. Chem. Phys.* **2015**, *17*, 32115–32121. [CrossRef]
9. Kanno, R.; Hata, T.; Kawamoto, Y.; Irie, M. Synthesis of a new lithium ionic conductor, thio-LISICON-lithium germanium sulfide system. *Solid State Ion.* **2000**, *130*, 97–104. [CrossRef]
10. Yao, P.; Zhu, B.; Zhai, H.; Liao, X.; Zhu, Y.; Xu, W.; Cheng, Q.; Jayyosi, C.; Li, Z.; Zhu, J.; et al. PVDF/Palygorskite Nanowire Composite Electrolyte for 4 V Rechargeable Lithium Batteries with High Energy Density. *Nano Lett.* **2018**, *18*, 6113–6120. [CrossRef]
11. Guo, Q.; Han, Y.; Wang, H.; Xiong, S.; Li, Y.; Liu, S.; Xie, K. New Class of LAGP-Based Solid Polymer Composite Electrolyte for Efficient and Safe Solid-State Lithium Batteries. *ACS Appl. Mater. Interfaces* **2017**, *9*, 41837–41844. [CrossRef]
12. Hu, H.; Cheng, H.; Liu, Z.; Li, G.; Zhu, Q.; Yu, Y. In Situ Polymerized PAN-Assisted S/C Nanosphere with Enhanced High-Power Performance as Cathode for Lithium/Sulfur Batteries. *Nano Lett.* **2015**, *15*, 5116–5123. [CrossRef]
13. Ahmad, S.; Saxena, T.K.; Ahmad, S.; Agnihotry, S.A. The effect of nanosized TiO_2 addition on poly(methylmethacrylate) based polymer electrolytes. *J. Power Sources* **2006**, *159*, 205–209. [CrossRef]
14. Li, L.; Deng, Y.; Chen, G. Status and prospect of garnet/polymer solid composite electrolytes for all-solid-state lithium batteries. *J. Energy Chem.* **2020**, *50*, 154–177. [CrossRef]
15. Costa, C.M.; Lizundia, E.; Lanceros-Méndez, S. Polymers for advanced lithium-ion batteries: State of the art and future needs on polymers for the different battery components. *Prog. Energy Combust. Sci.* **2020**, *79*, 100846. [CrossRef]
16. Wieczorek, W.; Zalewska, A.; Raducha, D.; Florjańczyk, Z.; Stevens, J.R. Composite Polyether Electrolytes with Lewis Acid Type Additives. *J. Phys. Chem. B* **1998**, *102*, 352–360. [CrossRef]
17. Fan, L.; Nan, C.-W.; Zhao, S. Effect of modified SiO_2 on the properties of PEO-based polymer electrolytes. *Solid State Ion.* **2003**, *164*, 81–86. [CrossRef]
18. Ward, I.M.; Hubbard, H.V.S.A. Polymer gel electrolytes: Conduction mechanism and battery applications. In *Ionic Interactions in Natural and Synthetic Macromolecules*; Wiley Online Library: Hoboken, NJ, USA, 2012; pp. 817–840.
19. Xu, K. Nonaqueous Liquid Electrolytes for Lithium-Based Rechargeable Batteries. *Chem. Rev.* **2004**, *104*, 4303–4418. [CrossRef] [PubMed]
20. Choi, S.W.; Jo, S.M.; Lee, W.S.; Kim, Y.-R. An Electrospun Poly(vinylidene fluoride) Nanofibrous Membrane and Its Battery Applications. *Adv. Mater.* **2003**, *15*, 2027–2032. [CrossRef]
21. Zhang, J.; Zeng, Y.; Li, Q.; Tang, Z.; Sun, D.; Huang, D.; Zhao, L.; Tang, Y.; Wang, H. Polymer-in-salt electrolyte enables ultrahigh ionic conductivity for advanced solid-state lithium metal batteries. *Energy Storage Mater.* **2023**, *54*, 440–449. [CrossRef]

22. Li, L.; Shan, Y.; Yang, X. New insights for constructing solid polymer electrolytes with ideal lithium-ion transfer channels by using inorganic filler. *Mater. Today Commun.* **2021**, *26*, 101910. [CrossRef]

23. Zeng, J.-P.; Liu, J.-F.; Huang, H.-D.; Shi, S.-C.; Kang, B.-H.; Dai, C.; Zhang, L.-W.; Yan, Z.-C.; Stadler, F.J.; He, Y.-B.; et al. A high polarity poly(vinylidene fluoride-co-trifluoroethylene) random copolymer with an all-trans conformation for solid-state LiNi$_{0.8}$Co$_{0.1}$Mn$_{0.1}$O$_2$/lithium metal batteries. *J. Mater. Chem. A* **2022**, *10*, 18061–18069. [CrossRef]

24. Liu, W.; Yi, C.; Li, L.; Liu, S.; Gui, Q.; Ba, D.; Li, Y.; Peng, D.; Liu, J. Designing Polymer-in-Salt Electrolyte and Fully Infiltrated 3D Electrode for Integrated Solid-State Lithium Batteries. *Angew. Chem. Int. Ed.* **2021**, *60*, 12931–12940. [CrossRef]

25. Ma, Y.; Zhou, Z.; Li, C.; Wang, L.; Wang, Y.; Cheng, X.; Zuo, P.; Du, C.; Huo, H.; Gao, Y.; et al. Enabling reliable lithium metal batteries by a bifunctional anionic electrolyte additive. *Energy Storage Mater.* **2018**, *11*, 197–204. [CrossRef]

26. Lu, D.; Shao, Y.; Lozano, T.; Bennett, W.D.; Graff, G.L.; Polzin, B.; Zhang, J.; Engelhard, M.H.; Saenz, N.T.; Henderson, W.A.; et al. Failure Mechanism for Fast-Charged Lithium Metal Batteries with Liquid Electrolytes. *Adv. Energy Mater.* **2015**, *5*, 1400993. [CrossRef]

27. Peled, E.; Golodnitsky, D.; Ardel, G. Advanced Model for Solid Electrolyte Interphase Electrodes in Liquid and Polymer Electrolytes. *J. Electrochem. Soc.* **1997**, *144*, L208. [CrossRef]

28. Pang, Q.; Liang, X.; Kochetkov, I.R.; Hartmann, P.; Nazar, L.F. Stabilizing Lithium Plating by a Biphasic Surface Layer Formed In Situ. *Angew. Chem. Int. Ed.* **2018**, *57*, 9795–9798. [CrossRef] [PubMed]

29. Zhang, X.-Q.; Cheng, X.-B.; Chen, X.; Yan, C.; Zhang, Q. Fluoroethylene Carbonate Additives to Render Uniform Li Deposits in Lithium Metal Batteries. *Adv. Funct. Mater.* **2017**, *27*, 1605989. [CrossRef]

30. Shen, X.; Ji, H.; Liu, J.; Zhou, J.; Yan, C.; Qian, T. Super lithiophilic SEI derived from quinones electrolyte to guide Li uniform deposition. *Energy Storage Mater.* **2020**, *24*, 426–431. [CrossRef]

31. Song, Z.; Qian, Y.; Liu, X.; Zhang, T.; Zhu, Y.; Yu, H.; Otani, M.; Zhou, H. A quinone-based oligomeric lithium salt for superior Li-organic batteries. *Energy Sci. Eng.* **2014**, *7*, 4077–4086. [CrossRef]